Differential exon usage and cryptic exon profiles of TDP-43 loss of function in amyotrophic lateral sclerosis brain tissue

Summary

TDP-43 dysfunction is a molecular hallmark of amyotrophic lateral sclerosis (ALS) and frontotemporal dementia (FTD). A major hypothesis of TDP-43 dysfunction in disease is the loss of normal nuclear function, resulting in impaired RNA regulation and the emergence of cryptic exons. Cryptic exons and exon changes are emerging as promising markers of lost TDP-43 function in addition to revealing biological pathways involved in neurodegeneration in ALS/FTD. Here, we investigated TDP-43 loss of function by depleting *TARDBP* from human post-mortem brain pericytes and identifying differential exon usage events with RNA-sequencing analysis. Differential exon usage events validated by qPCR were compiled into a panel with other well-established TDP-43 loss-of-function exon markers and then tested in ALS and control motor cortex tissue. We find that profiles of TDP-43-related cryptic exons and changed exon usage discriminate ALS brain tissue from controls, and propose that splicing panels may have predictive value for therapeutic intervention.

Introduction

Amyotrophic lateral sclerosis (ALS) and tau-negative frontotemporal dementia (FTD) represent the ends of a neurodegenerative spectrum characterized by TDP-43 proteinopathy (1-3). TDP-43 normally functions as an RNA binding protein in the nucleus, but in disease its misfolding and mislocalisation to the cytoplasm causes loss of nuclear function (4-6). Functions of TDP-43 that are lost in disease include RNA regulation and suppression of cryptic exons (7-11). As a result, the emergence of cryptic exons has become a promising marker of lost TDP-43 function and informs upon downstream events that lead to neurodegeneration in ALS/FTD. What is yet to be devised is a TDP-43-related 'exon usage panel' that could be utilised to gauge cellular dysfunction and the efficacy of therapeutic interventions. It will clearly be essential to validate that TDP-43-related cryptic exons and exon usage changes to be included in such a panel occur in ALS/FTD brain.

The normal physiological functions of TDP-43 involve the regulation of different stages of RNA metabolism, including the biogenesis, stability, degradation and splicing of coding and non-coding RNA (7, 8). TDP-43 has two RNA recognition motifs (RRM) that facilitate binding to RNA substrates, a nuclear localisation sequence (NLS) that allows nucleocytoplasmic transport and a glycine-rich C-terminus for protein-protein interactions (12). Several ALS-linked *TARDBP* mutation sites are concentrated in the glycine-rich region, encoded by exon 6, highlighting the importance of normal TDP-43 protein-protein binding (13). Nuclear TDP-43 autoregulates its own mRNA levels through binding its own 3' UTR (14), so loss of TDP-43 from the nucleus likely further contributes to TDP-43 overproduction, phase separation/aggregation, and sequestration (15-19). TDP-43 also regulates RNA splicing by suppressing or enhancing expression of exons (8-10, 12). Due to TDP-43 regulation of coding mRNAs that encode proteins of diverse and integral functions, numerous pathways may become impaired by dysfunctional TDP-43. This can result in global changes of gene expression that affect both ubiquitous and neuron-specific pathways (4). TDP-43 has been reported to bind to coding transcripts of various functions, including nucleocytoplasmic transport, neurotransmitter release, mitochondrial motility and microtubule stability (9, 10, 20-24). TDP-43 regulation of non-coding RNA can also have a significant effect on physiological processes. These include microRNAs (miRNA), long non-coding RNA (lncRNA), circular RNA (circRNA) and antisense RNA (asRNA), all of which can regulate mRNA expression (25). With the loss of normal physiological TDP-43 function, various downstream biological pathways may become dysregulated through changes in gene expression.

In addition to regulating mRNA expression levels, TDP-43 also regulates splicing, by suppressing or enhancing the expression of exons (8-10, 12). Recently, the role of TDP-43 as a suppressor of cryptic exons has been highlighted, particularly in the genes *STMN2* and *UNC13A* (21-24). Cryptic exons, interchangeably referred to as pseudoexons, usually result from errors during splicing that cause improper intron removal. Cryptic exons can also arise through cis-acting factors such as exon/intron boundaries or acceptor/donor splice sites being changed by single nucleotide polymorphisms (SNPs), or through the activity of trans-acting factors such as spliceosome proteins or RNA-binding proteins (26). Cryptic exons may alter the open reading frame and cause nonsense-mediated decay (NMD) of the mRNA by introducing a premature stop codon, which can mimic gene deletion (27). Trans-acting factors on cryptic exon inclusion are relatively understudied compared to cis-acting factors

(28), but several heterogenous nuclear ribonucleoproteins (hnRNPs) have been evidenced to regulate cryptic exon expression (29, 30). Thus, even without inherited SNPs, cryptic exons can emerge through RNA-binding protein dysfunction, as seen with loss of TDP-43 function (21-24).

Intriguingly, cryptic exons that emerge in human models of TDP-43 loss of function (LOF) and disease are generally not recapitulated in mouse models (4, 11, 31, 32). Therefore, because the role of TDP-43 is context dependent, human-derived transcriptomes are likely to be most suitable for identifying molecular pathways and drug targets relevant to human ALS/FTD. TDP-43 also has distinct sets of molecular targets within a given species but in different cell types (4, 11, 31, 32). While ALS is characterised by the degeneration of motor neurons, it is also recognised as a non-cell autonomous disorder, where non-neuronal cells contribute to neurodegeneration or accelerate disease progression (33-36). TDP-43 has previously been depleted from a range of different cell and tissue types to model disease, but the impact of TDP-43 LOF in non-neuronal cells is understudied. Here we examine TDP-43 LOF in primary human-brain derived pericyte cells.

Human brain pericytes are cells which encircle the endothelial cells of blood vessels, located on the abluminal side of the blood-brain barrier (BBB) and blood-spinal cord barrier (BSCB). Pericytes are critical to BBB integrity by stabilizing endothelial tight junctions and suppressing transcytosis across endothelia (37-40). In addition to being a critical contributor to BBB structural integrity, pericytes also have the ability to release cytokines that mediate leukocyte extravasation and propagate neuroinflammation (41-46), and the production of the cytokine IL-6 by pericytes is suppressed with TDP-43 knockdown (47). Loss of pericytes and breakdown of the BBB has been demonstrated in ALS patients and ALS animal models (40, 48-52). Indeed, pericytes are among the earliest cell types to show altered gene expression in the pre-symptomatic stage of ALS (53), suggesting they undergo cell-autonomous changes that do not depend on the degeneration of neurons. TDP-43 inclusions have not been detected in pericytes (54), but this does not rule out the possibility of TDP-43 dysfunction in pericytes. Further, these primary human brain-derived cells are an unmodified yet manipulable model for inducing TDP-43 LOF and understanding its impact on human transcriptomes.

In this study, we identified cryptic exons caused by TDP-43 LOF by bulk RNA sequencing of human brain-derived pericytes with siRNA-mediated TDP-43 depletion. We then examined the usage of our novel exon targets and previously reported exon targets in ALS brain tissue,

to determine whether profiles of differential exon usage and cryptic exons could contribute to ALS/FTD pathomechanisms and/or be harnessed as peripheral biomarkers or targets for intervention.

Results

Post-mortem human brain pericytes derived from the medial temporal gyrus (MTG) or motor cortex (MC) were isolated and treated with scrambled siRNA (scr) or siRNA against *TARDBP* (siTDP) to examine TDP-43 LOF. RNA samples were extracted from paired samples (scr and siTDP) from 12 donor cell lines (**Table S1**). Of these RNA samples, 9 pairs were sent for RNA-sequencing as reported previously (47) and 3 pairs (extracted from cell lines from different donors from those sent for sequencing) were used as a 'replication cohort' to validate RNA-sequencing results by qPCR. Successful TDP-43 depletion from the RNA-sequencing cohort was demonstrated by differential gene expression analysis using the *DESeq2* package in R software (**Fig. 1A**) and from the replication cohort by qPCR for *TARDBP* and immunocytochemistry for TDP-43 (**Fig. 1A, B**).

Differential exon usage (DEU) analysis of the RNA-sequencing data was performed using the *DEXSeq* package in R software. This package quantifies the relative usage of exonic elements, which are exons or parts of exons (annotated by feature ID, e.g. E001) and can therefore detect exon exclusion and exon inclusion; cryptic exon and intron retention events; as well as provide information on the non-coding elements of the transcript such as the 5' and 3' UTRs. A total of 1113 exonic elements were detected as differentially used after *TARDBP* knockdown in pericytes (padj < 0.05), and 6 DEU events of interest were selected from this dataset to validate by qPCR. Selection was based on the most significant padj values and exon expression (countData) in samples that either changed to or from very low expression level (<10 counts) with siTDP treatment (**Fig. 1C**). This would indicate that exonic element inclusion or exclusion was dependent on the presence of TDP-43. The 6 selected genes that showed such DEU events were *EXD3, DLG5, PAOX, NPHP4, B4GALT2* and *NYNRIN*. Additionally, 3 positive control genes that showed DEU events in the literature were tested: in *POLDIP3* (exon skipping (55)), *ATG4B* (cryptic exon (11, 56)) and *UNC13A* (retained intron (21)).

For the DEU events in these 9 genes, log2 fold-changes (log2FCs) in the replication cohort by qPCR were strongly correlated with log2FCs in the RNA-sequencing cohort by RNA-seq (**Fig. 1D,** R = 0.9193). Further, the directions of change in the DEU events in the RNA-sequencing cohort were validated in the replication cohort, with 6 genes (*POLDIP3, ATG4B, B4GALT2, NPHP4, EXD3* and *NYNRIN*) showing significantly different exon usage ($p < 0.05$) by qPCR (**Fig. 1E**).

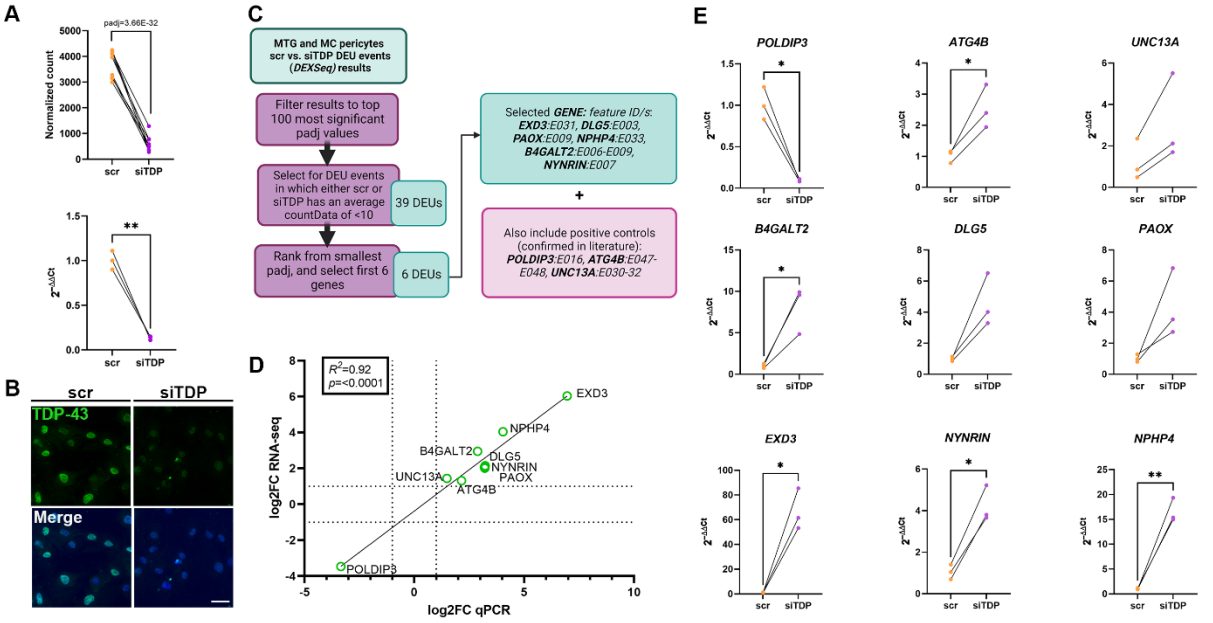

***Figure 1*: *Differential exon usage in human brain pericytes with TDP-43 knockdown*.** A) *TARDBP* depletion from pericytes was confirmed in the RNA-seq cohort by RNA-Seq (top, paired Wald test with Benjamini-Hochberg correction (padj = 3.66E-32)), and in the replication cohort by qPCR (bottom, paired t-test: **, p < 0.005). B) Depletion of TDP-43 protein levels was confirmed by immunocytochemistry of pericytes treated with scr or siTDP for 96 hours. Representative donor cell line shown. Scale bar, 50 µm. C) Flow chart showing the selection of DEU events of interest from DEU analysis to validate by qPCR. D) Correlation plot of log2FC determined by RNA-Seq and log2FC determined by qPCR of MTG and MC pericyte DEU events. Green points indicate the DEU event reached a log2FC of >1 or < -1. E) All DEU events (six from pericyte RNA-seq data and three from the literature) tested in the replication cohort by qPCR showed the same direction of change between scr and siTDP as the RNA-seq cohort. *POLDIP3, ATG4B, B4GALT2, NPHP4, EXD3* and *NYNRIN* were significantly changed (Paired t-test: *, p < 0.05; ** = 0.0086), and the other targets showed consistent direction and magnitude of change between biological replicates.

Following this, we generated a panel of TDP-43 LOF-induced DEU events to examine in human brain tissue (**Table 1**). These included DEU events identified in this study (DEU events from *B4GALT2, DLG5, EXD3, NPHP4, NYNRIN, PAOX*) and in our previous TDP-43 LOF meta-analysis (DEU events from *MMAB, IL18BP, GOSR2, MARK2, USP31, NDUFA5*) (4) along with positive controls previously tested in the literature (DEU events from *ATG4B, POLDIP3,* and *UNC13A* (as above), and *STMN2* (22, 24)).

Gene name	DEXSeq feature ID	Genomic location (GRCh38)	Change after TDP-43 KD
B4GALT2	E006-E009	43,979,877 - 43,980,046	increase
DLG5*	E003	77,793,544 - 77,794,007	increase

EXD3*	E031-E032	137,365,127 - 137,366,144	increase
NPHP4	E033	5,888,460 - 5,888,610	increase
NYNRIN	E007	24,412,594 - 24,412,691	increase
PAOX	E009	133,391,058 - 133,391,154	increase
GOSR2	E058	46,964,344 – 46,964,965	decrease
IL18BP	E033	72,002,805 – 72,003,753	decrease
MARK3	E067	103,503,361 – 103,503,826	increase
MMAB	E001	109,553,737 – 109,556,696	decrease
NDUFA5	E001	123,536,997 – 123,541,028	increase
USP31	E006	23,078,979 – 23,079,945	increase
ATG4B	E047-E048	241,668,686 - 241,670,725	increase
POLDIP3	E016-E017	42,601,970 – 42,602,107	decrease
STMN2	E001-E002	79,610,814 – 79,611,214	increase
UNC13A	E030-E032	17,627,941 – 17,628,337	increase

* DEU events from both this study in pericytes and TDP-43 LOF meta-analysis (4)

Table 1*: *Differential exon usage markers determined by TARDBP silencing in human brain pericytes and other human-derived cells. Non-shaded rows: DEU panel from TDP-43 LOF in pericytes (this study); light-shaded rows: DEU panel from TDP-43 LOF meta-analysis of various models (4); dark-shaded rows: DEU markers previously reported by TDP-43 LOF studies.

Fresh-frozen tissue samples from motor cortex of ten control (case IDs 'H#') and nine ALS cases (case IDs 'MN#') were obtained for RNA extraction, followed by cDNA synthesis and qPCR using primers to selectively amplify the DEU events. Age, sex and post-mortem delay were matched as closely as possible (**Table S2**). Primers to detect the cryptic exon in *STMN2,* usage of which is expected to increase with TDP-43 LOF and in ALS/FTD tissue, was included as a positive control (22, 24, 57) in addition to DEU/cryptic exons in *ATG4B, POLDIP3* and *UNC13A* .

The relative fold change ($2^{-\Delta\Delta Ct}$ method) for ALS samples and controls for each DEU event is presented in **Fig. 2A.** All DEU events tested could be detected within 40 PCR cycles except for that in *MMAB*. Therefore, Ct data for *MMAB* could not be obtained, presumably because *MMAB* gene expression was too low. While 3 DEU events were expected to show a decrease with TDP-43 LOF (*MMAB, IL18BP* and *GOSR2*), the mean $2^{-\Delta\Delta Ct}$ value for ALS cases was increased or trended towards an increase for almost all DEU events compared to controls. However, for the DEU events in *DLG5, NDUFA5, USP31* and *STMN2* which were predicted to increase, four cases in the ALS cohort (MN13, MN28, MN4 and MN9) demonstrated over

6-fold increases. Three of these DEU events (in *DLG5, NDUFA5* and *USP31*) were significantly increased in ALS tissue, as had been seen with TDP-43 LOF in pericyte RNA-seq data and/or meta-analysis of TDP-43 LOF models (4). Although positive controls did not show a significant increase in ALS samples, this may be due to the mixed cell-type nature of brain tissue.

When the ΔCts in each DEU event of the panel were considered together to represent a DEU/cryptic exon 'profile', principal component analysis (PCA) showed tight clustering of control cases, while ALS cases were more variable (**Fig. 2B**). Two control cases that clustered slightly apart from other controls (H230 and H190) had age-related changes indicated in their pathology reports (**Table S2**). Along the PC1 axis, MN4, MN9, MN13 and MN28 separated clearly from controls, while along the PC2 axis, MN38, MN5, MN31, MN23, MN13 and MN28 separated from controls, further supporting the finding that TDP-43 LOF DEU/cryptic exon profiles differ between individual ALS cases.

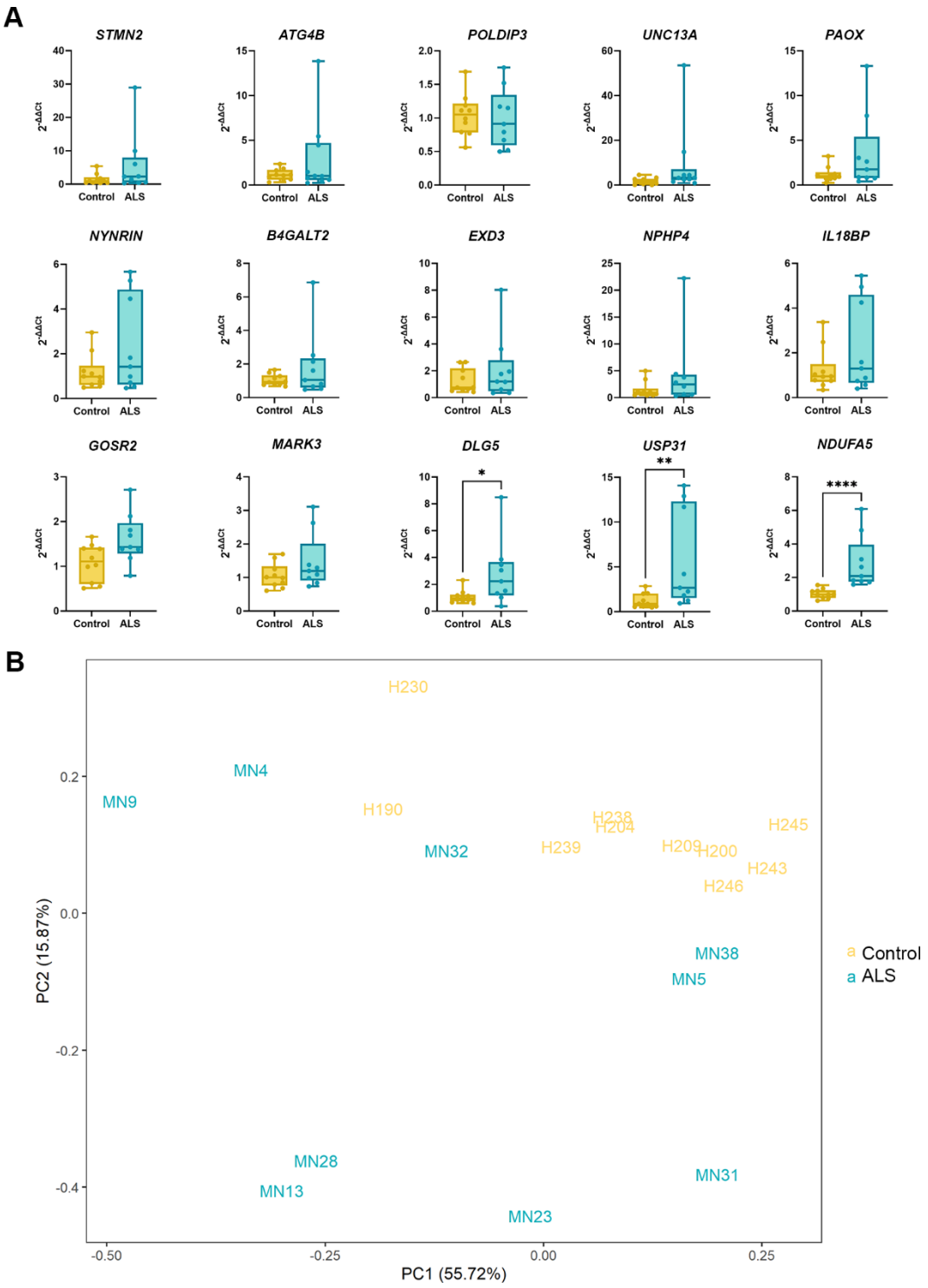

Figure 2*: *Detecting differential exon usage in ALS human brain tissue. A) Fold changes in DEU events between ALS and control motor cortex tissue by qPCR (Mann-Whitney U test: *, p = 0.035; **, p = 0.006 ; ****, p <0.0001). B) Principal component analysis of the ΔCt of each DEU event for each case. Yellow, control cases; blue, ALS cases.

Discussion

TDP-43 and splicing; a common target in ALS?

The heterogeneity in disease pathogenesis between individuals is one of the primary hurdles in ALS research. Determining common mechanisms of disease is challenging yet essential for developing therapeutics. Even with various genetic and environmental factors at play, the known common denominator in most ALS/FTD is TDP-43 proteinopathy (1, 2, 58). Therefore, understanding the events downstream of TDP-43 proteinopathy is likely to inform upon pathomechanisms that affect the largest patient population. Here we modelled TDP-43 LOF, which is caused by the interdependent processes of TDP-43 nuclear clearance (5, 59) and TDP-43 aggregation (2, 60). TDP-43 functions include splicing regulation and cryptic exon repression (9, 10) upon which the present study focuses. In testing the effects of TDP-43 LOF, we have identified key splicing events under regulatory control by TDP-43 and shown that the relative changes in these splicing events in tissue may differ between individuals with ALS.

Previous model systems for investigating loss of TDP-43 splicing function

Previous studies of TDP-43 splicing function indicated that a loss of TDP-43 function does not require its aggregation (8, 59), and that those splicing events are species and cell-type specific. For instance, cryptic exons resulting from TDP-43 depletion in a human-derived cell line did not concur with those in mouse embryonic stem cells, although mouse cells also underwent splicing changes (11, 32). We too observed species-specific splicing changes in our meta-analysis of transcriptomes following TDP-43 knockdown in various cell types (4). Further, within human models, there are cell-type-independent and cell-type-specific TDP-43 splicing targets (4), including in non-neuronal cell types such as Schwann cells and astrocytes that do not typically exhibit TDP-43 aggregation (61, 62). It is increasingly clear that identifying TDP-43 splicing targets in human disease requires human model systems, and that such targets may reveal TDP-43 dysfunction in neurons *and* other cell types even in the absence of TDP-43 aggregation.

Primary human brain pericytes with TDP-43 silencing for investigating loss of TDP-43 splicing function

We employed non-neuronal cultures of human brain origin to interrogate TDP-43 splicing targets: primary human post-mortem brain pericytes with TDP-43 silenced by siRNA. Pericytes are non-neuronal cells that degenerate in ALS, contributing to BBB leakage (40, 48-52). They are also among the first cell types of the brain to show signs of transcriptional changes in an ALS animal model (changes that were also observed in human ALS samples), suggesting cell-autonomous pericyte dysfunction despite the absence of TDP-43 aggregates (53, 54). In the present study, human brain pericytes were directly isolated from post-mortem brain tissue of multiple donors without reprogramming or transformation, thus incorporating donor-specific polymorphisms and retaining epigenetic signatures of ageing. Indeed, we found that human brain pericytes with TDP-43 depletion reliably recapitulated cryptic exon targets identified in previous studies in *POLDIP3*, *ATG4B*, and *UNC13A* (**Fig. 1E**), even though the expression of *UNC13A* is mainly neuronal (63-65).

TDP-43 splicing events in human brain pericytes

The top changed DEU/cryptic exons identified following TDP-43 knockdown in pericytes occurred in the genes *EXD3, DLG5, PAOX, NPHP4, B4GALT2* and *NYNRIN* (**Fig. 1C**), all of which were increased with TDP-43 knockdown. Events in *EXD3, DLG5, B4GALT2* and *NYNRIN* were also detectable in other human TDP-43 LOF models and/or TDP-negative neuronal nuclei from ALS/FTD tissue based on their RNA-Seq data (4), however only the cryptic exon in *DLG5* was significantly increased in ALS motor cortex tissue compared to controls in the present study. Brain tissue comprises various cell types, and both brain tissue sampling and disease can alter the relative proportions of cell types between samples. This variability will render DEU/cryptic exons difficult to detect if they only occur in a proportion of transcripts of that gene, a proportion of cells of a given cell type, or in rare cell types such as pericytes. Single-cell quantitative approaches should be used to discriminate between these possibilities for *EXD3, PAOX, NPHP4, B4GALT2* and *NYNRIN*, such as single-cell RNA sequencing (scRNA-seq) to compare DEU/cryptic exon events between cell types; RNA imaging technology in tissue such as RNAScope (66) in conjunction with cell-type markers; or using a combination of fluorescent *in situ* hybridization (FISH) and *in situ* sequencing such as Seq-Scope (67). Certainly, these splicing changes are reproducible across many TDP-43 LOF models and will report upon TDP-43 splicing function in suitable assays if not in bulk tissue.

TDP-43 splicing events in human ALS brain tissue

Significant DEU events that were validated in ALS brain tissue (identified following either TDP-43 knockdown in human brain pericytes or our previous meta-analysis of TDP-43 LOF studies) included exonic elements in the genes *USP31, NDUFA5* and *DLG5* (**Fig. 2A**); evidence that TDP-43 LOF is at least partially reflected in ALS tissue. The protein USP31 is involved in deubiquitylation (68); NDUFA5 is part of complex I of the mitochondrial respiratory chain (69); and DLG5 is a scaffold protein involved in cell polarity, cytoskeleton maintenance (70), microtubule stability (71) and synaptogenesis (72). The functions of these genes may be significant to pathomechanisms of disease. Tam and colleagues (73) analysed the transcriptomes of 148 ALS postmortem cortex samples and found that the majority (61%) displayed hallmarks of proteotoxic and oxidative stress, to which USP31 and NDUFA5 may contribute, given that deubiquitinating enzymes fine tune protein degradation (USP31 function) (74) and oxidative phosphorylation produces reactive oxygen species (NDUFA5 function) (75). The function of DLG5 may have parallels with other ALS-related genes involved in cytoskeletal dynamics such as *DCNT1* (76), *PFN1* (77, 78), *TUBA4A* (79) and *STMN2* (22, 24).

Based on the genomic location of the DEU events (**Table 1**), cryptic exon/retained intron events occur downstream of exon 13 for *USP31* and exon 25 for *DLG5*, while the exon usage change occurs at the 3'UTR for *NDUFA5*. The emergence of cryptic exons/retained introns may cause nonsense-mediated decay or altered translation, and 3'UTR alterations can result in a plethora of dysregulation possibilities, including altered mRNA stability, localisation, translation or interaction with other RNA-binding proteins (28, 80-83). The effects of these DEU events on the overall function of the genes in which they occur warrant further investigation. In addition to showing that TDP-43 LOF is evidenced in ALS tissue at the transcriptomic level, it will also be essential to determine cognate protein levels in ALS tissue to determine the translational and functional effect of TDP-43 LOF.

The variability in magnitude of individual DEU/cryptic exons (**Fig. 2A**) and the spread of combined DEU/cryptic exon 'profiles' by PCA (**Fig. 2B**) between brain tissues from different individuals suggests that heterogeneity in ALS may extend to TDP-43-related splicing changes. It is likely that the heterogeneity in DEU/cryptic exon expression in tissue is underpinned by the same factors, such as regional TDP-43 aggregate load (84) and genetic causes/ modifiers (85, 86), that drive clinical heterogeneity of ALS.

TDP-43 splicing events as biomarkers and therapeutic targets

Some DEU events have been proposed to have biomarker potential, such as a cryptic exon within *ATG4B* that emerged with TDP-43 LOF and in ALS (11, 56) as well as in Alzheimer's disease with TDP-43 pathology (59, 87). Diagnostic approaches include testing DEU changes or cryptic exon emergence with PCR or RNA-sequencing of biofluids (57, 88). Another emerging approach is designing aptamers or antibodies to cryptic peptides or neoepitopes that result from DEU events (89, 90). Indeed, the isoform switch of POLDIP3 from variant-1 to variant-2 due to exon skipping in *POLDIP3* has also been proposed to be a measurable protein biomarker due to variant-2 being rarely detected in normal tissues (55). Based on data from Genotype-Tissue Expression (GTEx) portal, genes *POLDIP3, ATG4B* and *MARK3* are the most ubiquitous, with relatively strong expression in whole blood as well (**Fig. S1**). Confirming whether DEU/cryptic exon events also occur in tissue accessible during life, such as blood and cerebral spinal fluid (CSF), will be necessary to determine their biomarker potential.

Correction of a cryptic exon in *UNC13A* caused by TDP-43 LOF has also been proposed as a treatment possibility, although this may be more effective or effective specifically in people with *UNC13A* polymorphisms (rs12608932 and rs12973192) that potentiate cryptic exon emergence with TDP-43 LOF (21, 23). We propose that specific profiles of DEU/cryptic exon events may contribute to and/or report on the heterogeneity in clinical manifestation of TDP-43 LOF. If individual DEU/cryptic exon profiles, tested using a panel such as the one presented here, are shown to predict treatment effect, such panels may be beneficial for stratifying ALS/FTD cases for personalised treatment.

Conclusion

Certain DEU/cryptic exon events that occur with TDP-43 LOF are recapitulated in ALS/FTD brain tissue, validating TDP-43 LOF as a disease mechanism. However, the magnitude of change of a given DEU/cryptic exon event varies between individuals. Further, because DEU/ cryptic exon events are enriched in specific cell types they are not always detectable in tissues of mixed cell type. TDP-43 LOF DEU/cryptic exon events will be useful as biomarkers if they also occur in readily accessible tissues such as blood or CSF. Correlating the DEU/cryptic exon 'profile' of an individual with their treatment response may then help tackle the challenge of disease heterogeneity by enabling stratification of treatment.

Methods

Donor pericyte line isolation, culture and transfection

All protocols involving human-derived samples were approved by the University of Auckland Human Participants Ethics Committee, and all methods were carried out in accordance with the approved guidelines. Post-mortem, non-neurodegenerative disease autopsy human brain tissue from 10 donors (7 male, 3 female; mean age 66.6 ± 13.5 years (SD)) was obtained from the Neurological Foundation Human Brain Bank (University of Auckland, New Zealand) (**Table S1**). Tissue from the middle temporal gyrus (MTG) and motor cortex (MC) was processed for the isolation of mixed glial cultures, with early passages (up to passage 5) containing a mixture of pericytes, astrocytes and microglia, as previously described (91). Cells were maintained as described previously (46, 47). Due to the proliferation of pericytes, which overgrow the non-proliferative glial cells, later passage cultures contain almost exclusively pericytes (43-45). To examine TDP-43 loss of function (LOF) in pericytes, cells were transfected with scrambled (scr) small interfering RNA (siRNA) or siRNA against *TARDBP* (siTDP) as described previously (47).

Donor human brain tissue

To validate whether splicing changes in pericytes with TDP-43 LOF were recapitulated in ALS, donor human brain tissue from control and ALS cases was examined. Cases were matched as closely as possible (**Table S2**). Control cases (6 male, 4 female; mean age 65.4 ± 11.4 years (SD)) were included in this study based on the absence of neurological conditions or significant neuropathologies. Age-related pathological changes were deemed acceptable. ALS cases (4 male, 5 female; mean age 62.2 ± 13.8 years (SD)) were included in this study based on a clinical diagnosis of ALS by neurologists at Auckland City or Middlemore Hospitals (New Zealand) during life. ALS pathology was confirmed by neuropathologists at Auckland City Hospital based on the detection of phosphorylated TDP-43 in the motor cortex and/or spinal cord post-mortem. The left hemispheres of donated brains obtained at autopsy were immediately dissected into functional blocks and frozen using CO_2 powder and stored at -80 °C as described previously (92). Fresh-frozen motor cortex tissue from sensory-motor cortex (SM) or motor cortex (MC) blocks (maximum input weight 20 mg) was used for RNA isolation.

RNA isolation and RNA-sequencing

Following 96 h transfection with siRNA (scr or siTDP), cells plated at 15,000 cells/cm^2 in 6-well plates were washed in ice-cold 1X phosphate-buffered saline (PBS) and RNA extraction and purification was performed using the RNAqueous®-Micro Total RNA isolation Kit (Ambion) as per manufacturer's instructions. RNA isolation from fresh-frozen brain tissue was performed using the RNeasy® Mini kit as per manufacturer's instructions. To homogenise the tissue, it was first disrupted in 600 µL lysis buffer (Buffer RLT) using pre-chilled pestles then passed through a 23-gauge needle 10 times. RNA integrity (RNA integrity number; RIN) was assessed using the Agilent RNA 6000 Pico Kit (Agilent Technologies) on an Agilent 2100 Bioanalyzer (Agilent Technologies). RNA from paired samples (scr and siTDP) from 9 donor cell lines (**Table S1**) were sent to AnnoRoad Gene Technology (Beijing, China) for quality check, library preparations and sequencing using the Illumina NovaSeq6000 platform and analysed as described previously (4, 47). Reads were aligned to the GRCh38 reference genome with HISAT2 (93) and quantified with StringTie (94). R package *DESeq2* (95) was used for differential expression analysis and *DEXSeq* (96) was used for exon usage analysis.

Quantitative reverse transcription PCR (qPCR) and primer design

To validate DEGs and DEU events detected by RNA-sequencing, RNA from three pairs of pericyte cases, considered a 'replication cohort' (**Table S1**), was tested by qPCR. Either 0.5 or 1 µg of RNA was used for cDNA synthesis. RNA was treated with DNase I (Promega) (1 µg DNase I/ 1 µg RNA) and cDNA was synthesised using a Superscript® First-Strand Synthesis IV kit (ThermoFisher Scientific). QPCR was performed with Platinum® SYBR® Green qPCR SuperMix-UDG with Rox (ThermoFisher Scientific) with a QuantStudio™ 12K Flex Real-Time PCR system (Applied Biosystems). The qPCR program was set to 50 °C for 2 min, 95 °C for 10 min, and 40 cycles of 95 °C for 15 s and 60 °C for 1 min. Relative quantification was determined using the delta-delta Ct method with normalization to the housekeeping gene *GAPDH*. The fold changes are reported using $2^{-\Delta\Delta Ct}$ values, with the ΔCt for each case calculated relative to the average ΔCt of all control cases.

Primers were designed using PrimerBlast and Geneious 10.2.6 software (97). PrimerBlast parameters were set to 80-120 bp amplicon length, maximum primer T_m difference 2 °C, and GC content 50%-60%. Maximum self-complementarity was set to 4 and self-3' complementarity was set to 2. Primer sequences can be found in **Table S3**.

Immunocytochemistry and image acquisition

To confirm the extent of TDP-43 silencing in human brain pericytes, following 96 h transfection with siRNA (scr or siTDP), cells plated at 15,000 cells/cm^2 in 96-well plates were fixed in 4% PFA for 10 minutes and washed in 1X PBS containing 0.2% (v/v) Triton X-100 (PBS-T). Cells were incubated with rabbit polyclonal anti-TDP-43 (1078-2-2-AP, Proteintech) diluted 1:2000 in PBS-T with 1% goat serum overnight at 4 °C. Cells were then washed twice with 1X PBS and incubated with goat anti-rabbit AlexaFluor™ Plus 488 (A32731, ThermoFisher Scientific) diluted 1:500 in PBS-T with 1% goat serum overnight at 4 °C. Cells were then washed twice with 1X PBS and nuclei were counterstained with 20 nM Hoechst 33258 (Sigma-Aldrich) diluted in PBS-T for 10 minutes. Images of immuno-stained cells were acquired using an Image Xpress Micro XLS High Content Screening system (Molecular Devices) at 10X/0.3 NA Plan Fluor magnification using filters DAPI (excitation range 381-399 nm) and FITC (excitation range 474-496 nm).

Publicly available data

Gene expression heatmap displaying genes with DEU events from TDP-43 LOF was obtained from the Genotype-Tissue Expression (GTEx) Portal V8 (www.gtexportal.org) on 09 January 2023 (dbGaP accession number phs000424.v9.p2) using the Multi-Gene Query .

Statistical analysis

Statistical analysis for differential exon usage was performed by the R package *DEXSeq*, which used *DESeq2* Wald test and false discovery correction with Benjamini-Hochberg method (95, 96). Significant padj value was set to <0.05. Paired t-test was performed for scr versus siTDP pericyte comparisons, whilst Mann-Whitney U test was performed for control versus ALS brain tissue comparisons, using GraphPad Prism 9.0 software (La Jolla, CA, USA). Significant p value was set to <0.05. Principal component analysis (PCA) was performed for each control and ALS case based on the ΔCT values for each RT-qPCR primer pair using the prcomp function within R software.

Acknowledgements

This publication is dedicated to the patients and families who contribute to our research. This work was supported by grants from Motor Neuron Disease NZ, Freemasons New Zealand,

Matteo de Nora, Coker Family Trust, Sir Thomas and Lady Duncan Trust, Hugh Green Foundation and PaR NZ Golfing.

References

1. Arai T, Hasegawa M, Akiyama H, Ikeda K, Nonaka T, Mori H, et al. TDP-43 is a component of ubiquitin-positive tau-negative inclusions in frontotemporal lobar degeneration and amyotrophic lateral sclerosis. Biochem Biophys Res Commun. 2006;351(3):602-11.
2. Neumann M, Sampathu DM, Kwong LK, Truax AC, Micsenyi MC, Chou TT, et al. Ubiquitinated TDP-43 in frontotemporal lobar degeneration and amyotrophic lateral sclerosis. Science. 2006;314(5796):130-3.
3. Ling SC, Polymenidou M, Cleveland DW. Converging mechanisms in ALS and FTD: disrupted RNA and protein homeostasis. Neuron. 2013;79(3):416-38.
4. Cao MC, Scotter EL. Transcriptional targets of amyotrophic lateral sclerosis/frontotemporal dementia protein TDP-43 - meta-analysis and interactive graphical database. Dis Model Mech. 2022;15(9).
5. Liu EY, Russ J, Cali CP, Phan JM, Amlie-Wolf A, Lee EB. Loss of nuclear TDP-43 is associated with decondensation of LINE retrotransposons. Cell reports. 2019;27(5):1409-21. e6.
6. Lee EB, Lee VM, Trojanowski JQ. Gains or losses: molecular mechanisms of TDP43-mediated neurodegeneration. Nat Rev Neurosci. 2011;13(1):38-50.
7. De Conti L, Akinyi MV, Mendoza-Maldonado R, Romano M, Baralle M, Buratti E. TDP-43 affects splicing profiles and isoform production of genes involved in the apoptotic and mitotic cellular pathways. Nucleic Acids Res. 2015;43(18):8990-9005.
8. Arnold ES, Ling SC, Huelga SC, Lagier-Tourenne C, Polymenidou M, Ditsworth D, et al. ALS-linked TDP-43 mutations produce aberrant RNA splicing and adult-onset motor neuron disease without aggregation or loss of nuclear TDP-43. Proc Natl Acad Sci U S A. 2013;110(8):E736-45.
9. Polymenidou M, Lagier-Tourenne C, Hutt KR, Huelga SC, Moran J, Liang TY, et al. Long pre-mRNA depletion and RNA missplicing contribute to neuronal vulnerability from loss of TDP-43. Nat Neurosci. 2011;14(4):459-68.
10. Tollervey JR, Curk T, Rogelj B, Briese M, Cereda M, Kayikci M, et al. Characterizing the RNA targets and position-dependent splicing regulation by TDP-43. Nat Neurosci. 2011;14(4):452-8.
11. Ling JP, Pletnikova O, Troncoso JC, Wong PC. TDP-43 repression of nonconserved cryptic exons is compromised in ALS-FTD. Science. 2015;349(6248):650-5.
12. Buratti E, Baralle FE. Characterization and functional implications of the RNA binding properties of nuclear factor TDP-43, a novel splicing regulator of CFTR exon 9. J Biol Chem. 2001;276(39):36337-43.
13. Pesiridis GS, Lee VM, Trojanowski JQ. Mutations in TDP-43 link glycine-rich domain functions to amyotrophic lateral sclerosis. Hum Mol Genet. 2009;18(R2):R156-62.
14. Ayala YM, De Conti L, Avendaño-Vázquez SE, Dhir A, Romano M, D'ambrogio A, et al. TDP-43 regulates its mRNA levels through a negative feedback loop. The EMBO journal. 2011;30(2):277-88.
15. Tziortzouda P, Van Den Bosch L, Hirth F. Triad of TDP43 control in neurodegeneration: autoregulation, localization and aggregation. Nat Rev Neurosci. 2021.
16. Amlie-Wolf A, Ryvkin P, Tong R, Dragomir I, Suh E, Xu Y, et al. Transcriptomic Changes Due to Cytoplasmic TDP-43 Expression Reveal Dysregulation of Histone Transcripts and Nuclear Chromatin. PLoS One. 2015;10(10):e0141836.
17. Mutihac R, Alegre-Abarrategui J, Gordon D, Farrimond L, Yamasaki-Mann M, Talbot K, et al. TARDBP pathogenic mutations increase cytoplasmic translocation of TDP-43 and cause reduction of endoplasmic reticulum Ca(2)(+) signaling in motor neurons. Neurobiol Dis. 2015;75:64-77.
18. Walker AK, Spiller KJ, Ge G, Zheng A, Xu Y, Zhou M, et al. Functional recovery in new mouse models of ALS/FTLD after clearance of pathological cytoplasmic TDP-43. Acta Neuropathol. 2015;130(5):643-60.

19. Winton MJ, Igaz LM, Wong MM, Kwong LK, Trojanowski JQ, Lee VM. Disturbance of nuclear and cytoplasmic TAR DNA-binding protein (TDP-43) induces disease-like redistribution, sequestration, and aggregate formation. J Biol Chem. 2008;283(19):13302-9.
20. Sephton CF, Cenik C, Kucukural A, Dammer EB, Cenik B, Han Y, et al. Identification of neuronal RNA targets of TDP-43-containing ribonucleoprotein complexes. J Biol Chem. 2011;286(2):1204-15.
21. Brown AL, Wilkins OG, Keuss MJ, Hill SE, Zanovello M, Lee WC, et al. TDP-43 loss and ALS-risk SNPs drive mis-splicing and depletion of UNC13A. Nature. 2022;603(7899):131-7.
22. Klim JR, Williams LA, Limone F, Guerra San Juan I, Davis-Dusenbery BN, Mordes DA, et al. ALS-implicated protein TDP-43 sustains levels of STMN2, a mediator of motor neuron growth and repair. Nat Neurosci. 2019;22(2):167-79.
23. Ma XR, Prudencio M, Koike Y, Vatsavayai SC, Kim G, Harbinski F, et al. TDP-43 represses cryptic exon inclusion in the FTD-ALS gene UNC13A. Nature. 2022;603(7899):124-30.
24. Melamed Ze, López-Erauskin J, Baughn MW, Zhang O, Drenner K, Sun Y, et al. Premature polyadenylation-mediated loss of stathmin-2 is a hallmark of TDP-43-dependent neurodegeneration. Nature neuroscience. 2019;22(2):180-90.
25. Esteller M. Non-coding RNAs in human disease. Nat Rev Genet. 2011;12(12):861-74.
26. Abramowicz A, Gos M. Correction to: Splicing mutations in human genetic disorders: examples, detection, and confirmation. J Appl Genet. 2019;60(2):231.
27. Sterne-Weiler T, Sanford JR. Exon identity crisis: disease-causing mutations that disrupt the splicing code. Genome Biol. 2014;15(1):201.
28. Dhir A, Buratti E. Alternative splicing: role of pseudoexons in human disease and potential therapeutic strategies. FEBS J. 2010;277(4):841-55.
29. Coles JL, Hallegger M, Smith CW. A nonsense exon in the Tpm1 gene is silenced by hnRNP H and F. RNA. 2009;15(1):33-43.
30. Spellman R, Smith CW. Novel modes of splicing repression by PTB. Trends Biochem Sci. 2006;31(2):73-6.
31. Humphrey J, Emmett W, Fratta P, Isaacs AM, Plagnol V. Quantitative analysis of cryptic splicing associated with TDP-43 depletion. BMC Med Genomics. 2017;10(1):38.
32. Jeong YH, Ling JP, Lin SZ, Donde AN, Braunstein KE, Majounie E, et al. Tdp-43 cryptic exons are highly variable between cell types. Molecular neurodegeneration. 2017;12(1):13.
33. Corcia P, Tauber C, Vercoullie J, Arlicot N, Prunier C, Praline J, et al. Molecular imaging of microglial activation in amyotrophic lateral sclerosis. PLoS One. 2012;7(12):e52941.
34. Schiffer D, Cordera S, Cavalla P, Migheli A. Reactive astrogliosis of the spinal cord in amyotrophic lateral sclerosis. J Neurol Sci. 1996;139 Suppl:27-33.
35. Kang SH, Li Y, Fukaya M, Lorenzini I, Cleveland DW, Ostrow LW, et al. Degeneration and impaired regeneration of gray matter oligodendrocytes in amyotrophic lateral sclerosis. Nat Neurosci. 2013;16(5):571-9.
36. Philips T, Rothstein JD. Glial cells in amyotrophic lateral sclerosis. Exp Neurol. 2014;262 Pt B:111-20.
37. Geranmayeh MH, Rahbarghazi R, Farhoudi M. Targeting pericytes for neurovascular regeneration. Cell Commun Signal. 2019;17(1):26.
38. Daneman R, Zhou L, Kebede AA, Barres BA. Pericytes are required for blood-brain barrier integrity during embryogenesis. Nature. 2010;468(7323):562-6.
39. Winkler EA, Sengillo JD, Bell RD, Wang J, Zlokovic BV. Blood-spinal cord barrier pericyte reductions contribute to increased capillary permeability. J Cereb Blood Flow Metab. 2012;32(10):1841-52.
40. Armulik A, Genove G, Mae M, Nisancioglu MH, Wallgard E, Niaudet C, et al. Pericytes regulate the blood-brain barrier. Nature. 2010;468(7323):557-61.
41. Jansson D, Rustenhoven J, Feng S, Hurley D, Oldfield RL, Bergin PS, et al. A role for human brain pericytes in neuroinflammation. J Neuroinflammation. 2014;11:104.

42. Rustenhoven J, Aalderink M, Scotter EL, Oldfield RL, Bergin PS, Mee EW, et al. TGF-beta1 regulates human brain pericyte inflammatory processes involved in neurovasculature function. J Neuroinflammation. 2016;13:37.
43. Rustenhoven J, Scotter EL, Jansson D, Kho DT, Oldfield RL, Bergin PS, et al. An anti-inflammatory role for C/EBPdelta in human brain pericytes. Sci Rep. 2015;5:12132.
44. Smyth LCD, Rustenhoven J, Park TI, Schweder P, Jansson D, Heppner PA, et al. Unique and shared inflammatory profiles of human brain endothelia and pericytes. J Neuroinflammation. 2018;15(1):138.
45. Rustenhoven J, Jansson D, Smyth LC, Dragunow M. Brain Pericytes As Mediators of Neuroinflammation. Trends Pharmacol Sci. 2017;38(3):291-304.
46. Cao MC, Cawston EE, Chen G, Brooks C, Douwes J, McLean D, et al. Serum biomarkers of neuroinflammation and blood-brain barrier leakage in amyotrophic lateral sclerosis. BMC Neurol. 2022;22(1):216.
47. Scotter EL, Cao MC, Jansson D, Rustenhoven J, Smyth LCD, Aalderink MC, et al. The amyotrophic lateral sclerosis-linked protein TDP-43 regulates interleukin-6 cytokine production by human brain pericytes. Mol Cell Neurosci. 2022;123:103768.
48. Bell RD, Winkler EA, Sagare AP, Singh I, LaRue B, Deane R, et al. Pericytes control key neurovascular functions and neuronal phenotype in the adult brain and during brain aging. Neuron. 2010;68(3):409-27.
49. Garbuzova-Davis S, Hernandez-Ontiveros DG, Rodrigues MC, Haller E, Frisina-Deyo A, Mirtyl S, et al. Impaired blood-brain/spinal cord barrier in ALS patients. Brain Res. 2012;1469:114-28.
50. Sasaki S, Iguchi Y, Katsuno M, Sobue G. Alterations in the blood-spinal cord barrier in TDP-43 conditional knockout mice. Neurosci Lett. 2015;598:1-5.
51. Winkler EA, Sengillo JD, Sullivan JS, Henkel JS, Appel SH, Zlokovic BV. Blood-spinal cord barrier breakdown and pericyte reductions in amyotrophic lateral sclerosis. Acta Neuropathol. 2013;125(1):111-20.
52. Yamadera M, Fujimura H, Inoue K, Toyooka K, Mori C, Hirano H, et al. Microvascular disturbance with decreased pericyte coverage is prominent in the ventral horn of patients with amyotrophic lateral sclerosis. Amyotroph Lateral Scler Frontotemporal Degener. 2015;16(5-6):393-401.
53. Manberg A, Skene N, Sanders F, Trusohamn M, Remnestal J, Szczepinska A, et al. Altered perivascular fibroblast activity precedes ALS disease onset. Nat Med. 2021;27(4):640-6.
54. Nolan M, Scott C, Gamarallage MP, Lunn D, Carpenter K, McDonough E, et al. Quantitative patterns of motor cortex proteinopathy across ALS genotypes. Acta neuropathologica communications. 2020;8(1):98.
55. Shiga A, Ishihara T, Miyashita A, Kuwabara M, Kato T, Watanabe N, et al. Alteration of POLDIP3 splicing associated with loss of function of TDP-43 in tissues affected with ALS. PLoS One. 2012;7(8):e43120.
56. Torres P, Ramirez-Nunez O, Romero-Guevara R, Bares G, Granado-Serrano AB, Ayala V, et al. Cryptic exon splicing function of TARDBP interacts with autophagy in nervous tissue. Autophagy. 2018;14(8):1398-403.
57. Prudencio M, Humphrey J, Pickles S, Brown AL, Hill SE, Kachergus JM, et al. Truncated stathmin-2 is a marker of TDP-43 pathology in frontotemporal dementia. J Clin Invest. 2020;130(11):6080-92.
58. Geser F, Lee VM, Trojanowski JQ. Amyotrophic lateral sclerosis and frontotemporal lobar degeneration: a spectrum of TDP-43 proteinopathies. Neuropathology. 2010;30(2):103-12.
59. Sun M, Bell W, LaClair KD, Ling JP, Han H, Kageyama Y, et al. Cryptic exon incorporation occurs in Alzheimer's brain lacking TDP-43 inclusion but exhibiting nuclear clearance of TDP-43. Acta Neuropathol. 2017;133(6):923-31.

60. Yang C, Tan W, Whittle C, Qiu L, Cao L, Akbarian S, et al. The C-terminal TDP-43 fragments have a high aggregation propensity and harm neurons by a dominant-negative mechanism. PLoS One. 2010;5(12):e15878.
61. Chang KJ, Agrawal I, Vainshtein A, Ho WY, Xin W, Tucker-Kellogg G, et al. TDP-43 maximizes nerve conduction velocity by repressing a cryptic exon for paranodal junction assembly in Schwann cells. Elife. 2021;10.
62. Ziff OJ, Taha DM, Crerar H, Clarke BE, Chakrabarti AM, Kelly G, et al. Reactive astrocytes in ALS display diminished intron retention. Nucleic Acids Res. 2021;49(6):3168-84.
63. Deng L, Kaeser PS, Xu W, Sudhof TC. RIM proteins activate vesicle priming by reversing autoinhibitory homodimerization of Munc13. Neuron. 2011;69(2):317-31.
64. Augustin I, Rosenmund C, Sudhof TC, Brose N. Munc13-1 is essential for fusion competence of glutamatergic synaptic vesicles. Nature. 1999;400(6743):457-61.
65. Lipstein N, Verhoeven-Duif NM, Michelassi FE, Calloway N, van Hasselt PM, Pienkowska K, et al. Synaptic UNC13A protein variant causes increased neurotransmission and dyskinetic movement disorder. J Clin Invest. 2017;127(3):1005-18.
66. Wang F, Flanagan J, Su N, Wang LC, Bui S, Nielson A, et al. RNAscope: a novel in situ RNA analysis platform for formalin-fixed, paraffin-embedded tissues. J Mol Diagn. 2012;14(1):22-9.
67. Cho CS, Xi J, Si Y, Park SR, Hsu JE, Kim M, et al. Microscopic examination of spatial transcriptome using Seq-Scope. Cell. 2021;184(13):3559-72 e22.
68. Lockhart PJ, Hulihan M, Lincoln S, Hussey J, Skipper L, Bisceglio G, et al. Identification of the human ubiquitin specific protease 31 (USP31) gene: structure, sequence and expression analysis. DNA Seq. 2004;15(1):9-14.
69. Loeffen JL, Triepels RH, van den Heuvel LP, Schuelke M, Buskens CA, Smeets RJ, et al. cDNA of eight nuclear encoded subunits of NADH:ubiquinone oxidoreductase: human complex I cDNA characterization completed. Biochem Biophys Res Commun. 1998;253(2):415-22.
70. Liu J, Li J, Ren Y, Liu P. DLG5 in cell polarity maintenance and cancer development. Int J Biol Sci. 2014;10(5):543-9.
71. Kwan J, Sczaniecka A, Heidary Arash E, Nguyen L, Chen CC, Ratkovic S, et al. DLG5 connects cell polarity and Hippo signaling protein networks by linking PAR-1 with MST1/2. Genes Dev. 2016;30(24):2696-709.
72. Wang SH, Celic I, Choi SY, Riccomagno M, Wang Q, Sun LO, et al. Dlg5 regulates dendritic spine formation and synaptogenesis by controlling subcellular N-cadherin localization. J Neurosci. 2014;34(38):12745-61.
73. Tam OH, Rozhkov NV, Shaw R, Kim D, Hubbard I, Fennessey S, et al. Postmortem Cortex Samples Identify Distinct Molecular Subtypes of ALS: Retrotransposon Activation, Oxidative Stress, and Activated Glia. Cell Rep. 2019;29(5):1164-77 e5.
74. Tzimas C, Michailidou G, Arsenakis M, Kieff E, Mosialos G, Hatzivassiliou EG. Human ubiquitin specific protease 31 is a deubiquitinating enzyme implicated in activation of nuclear factor-kappaB. Cell Signal. 2006;18(1):83-92.
75. Rak M, Rustin P. Supernumerary subunits NDUFA3, NDUFA5 and NDUFA12 are required for the formation of the extramembrane arm of human mitochondrial complex I. FEBS Lett. 2014;588(9):1832-8.
76. Munch C, Rosenbohm A, Sperfeld AD, Uttner I, Reske S, Krause BJ, et al. Heterozygous R1101K mutation of the DCTN1 gene in a family with ALS and FTD. Ann Neurol. 2005;58(5):777-80.
77. Wu CH, Fallini C, Ticozzi N, Keagle PJ, Sapp PC, Piotrowska K, et al. Mutations in the profilin 1 gene cause familial amyotrophic lateral sclerosis. Nature. 2012;488(7412):499-503.
78. Smith BN, Vance C, Scotter EL, Troakes C, Wong CH, Topp S, et al. Novel mutations support a role for Profilin 1 in the pathogenesis of ALS. Neurobiol Aging. 2015;36(3):1602 e17-27.
79. Smith BN, Ticozzi N, Fallini C, Gkazi AS, Topp S, Kenna KP, et al. Exome-wide rare variant analysis identifies TUBA4A mutations associated with familial ALS. Neuron. 2014;84(2):324-31.

80. Berkovits BD, Mayr C. Alternative 3' UTRs act as scaffolds to regulate membrane protein localization. Nature. 2015;522(7556):363-7.
81. Macdonald PM, Struhl G. cis-acting sequences responsible for anterior localization of bicoid mRNA in Drosophila embryos. Nature. 1988;336(6199):595-8.
82. Meijlink F, Curran T, Miller AD, Verma IM. Removal of a 67-base-pair sequence in the noncoding region of protooncogene fos converts it to a transforming gene. Proc Natl Acad Sci U S A. 1985;82(15):4987-91.
83. Miller GM, Madras BK. Polymorphisms in the 3'-untranslated region of human and monkey dopamine transporter genes affect reporter gene expression. Mol Psychiatry. 2002;7(1):44-55.
84. Brettschneider J, Del Tredici K, Toledo JB, Robinson JL, Irwin DJ, Grossman M, et al. Stages of pTDP-43 pathology in amyotrophic lateral sclerosis. Ann Neurol. 2013;74(1):20-38.
85. McCann EP, Williams KL, Fifita JA, Tarr IS, O'Connor J, Rowe DB, et al. The genotype-phenotype landscape of familial amyotrophic lateral sclerosis in Australia. Clin Genet. 2017;92(3):259-66.
86. Witzel S, Wagner M, Zhao C, Kandler K, Graf E, Berutti R, et al. Fast versus slow disease progression in amyotrophic lateral sclerosis-clinical and genetic factors at the edges of the survival spectrum. Neurobiol Aging. 2022;119:117-26.
87. Torres P, Andres-Benito P, Fernandez-Bernal A, Ricart M, Ayala V, Pamplona R, et al. Selected cryptic exons accumulate in hippocampal cell nuclei in Alzheimer's disease with and without associated TDP-43 proteinopathy. Brain. 2020;143(3):e20.
88. Koh W, Pan W, Gawad C, Fan HC, Kerchner GA, Wyss-Coray T, et al. Noninvasive in vivo monitoring of tissue-specific global gene expression in humans. Proc Natl Acad Sci U S A. 2014;111(20):7361-6.
89. Seddighi S, Qi YA, Brown A-L, Wilkins OG, Bereda C, Belair C, et al. Mis-spliced transcripts generate de novo proteins in TDP-43-related ALS/FTD. 2023:2023.01.23.525149.
90. Irwin KE, Jasin P, Braunstein KE, Sinha I, Bowden KD, Moghekar A, et al. A fluid biomarker reveals loss of TDP-43 splicing repression in pre-symptomatic ALS. 2023:2023.01.23.525202.
91. Gibbons HM, Hughes SM, Van Roon-Mom W, Greenwood JM, Narayan PJ, Teoh HH, et al. Cellular composition of human glial cultures from adult biopsy brain tissue. J Neurosci Methods. 2007;166(1):89-98.
92. Waldvogel HJ, Bullock JY, Synek BJ, Curtis MA, van Roon-Mom WM, Faull RL. The collection and processing of human brain tissue for research. Cell Tissue Bank. 2008;9(3):169-79.
93. Kim D, Paggi JM, Park C, Bennett C, Salzberg SL. Graph-based genome alignment and genotyping with HISAT2 and HISAT-genotype. Nat Biotechnol. 2019;37(8):907-15.
94. Pertea M, Kim D, Pertea GM, Leek JT, Salzberg SL. Transcript-level expression analysis of RNA-seq experiments with HISAT, StringTie and Ballgown. Nat Protoc. 2016;11(9):1650-67.
95. Love MI, Huber W, Anders S. Moderated estimation of fold change and dispersion for RNA-seq data with DESeq2. Genome Biol. 2014;15(12):550.
96. Anders S, Reyes A, Huber W. Detecting differential usage of exons from RNA-seq data. Genome Res. 2012;22(10):2008-17.
97. Kearse M, Moir R, Wilson A, Stones-Havas S, Cheung M, Sturrock S, et al. Geneious Basic: an integrated and extendable desktop software platform for the organization and analysis of sequence data. Bioinformatics. 2012;28(12):1647-9.